

Finding the remnants of the Milky Way’s last neutron star mergers

MENG-RU WU,^{1,2} PROJJWAL BANERJEE,^{3,4} BRIAN D. METZGER,⁵ GABRIEL MARTÍNEZ-PINEDO,^{6,7} TSUGUO ARAMAKI,⁸
ERIC BURNS,⁹ CHARLES J. HAILEY,¹⁰ JENNIFER BARNES,^{10,*} AND GEORGIA KARAGIORGI¹¹

¹*Institute of Physics, Academia Sinica, Taipei, 11529, Taiwan; mwu@gate.sinica.edu.tw*

²*Institute of Astronomy and Astrophysics, Academia Sinica, Taipei, 10617, Taiwan*

³*Department of Astronomy, School of Physics and Astronomy, Shanghai Jiao Tong University, Shanghai 200240, China; projjwal.banerjee@gmail.com*

⁴*Department of Physics, Indian Institute of Technology Palakkad, Palakkad, Kerala 678557, India*

⁵*Department of Physics and Columbia Astrophysics Laboratory, Columbia University, Pupin Hall, New York, NY 10027, USA; bdm2129@columbia.edu*

⁶*GSI Helmholtzzentrum für Schwerionenforschung, 64291 Darmstadt, Germany*

⁷*Institut für Kernphysik (Theoriezentrum), Technische Universität Darmstadt, 64289 Darmstadt, Germany*

⁸*SLAC National Accelerator Laboratory/Kavli Institute for Particle Astrophysics and Cosmology, Menlo Park, CA 94025, USA*

⁹*NASA Postdoctoral Program Fellow, Goddard Space Flight Center, Greenbelt, MD 20771, USA*

¹⁰*Department of Physics and Columbia Astrophysics Laboratory, Columbia University, Pupin Hall, New York, NY 10027, USA*

¹¹*Department of Physics, Columbia University, Pupin Hall, New York, NY 10027, USA*

(Dated: February 19, 2024)

ABSTRACT

The discovery of a binary neutron star merger (NSM) through both its gravitational wave and electromagnetic emission has revealed these events to be key sites of r -process nucleosynthesis. Here, we evaluate the prospects of finding the remnants of Galactic NSMs by detecting the gamma-ray decay lines from their radioactive r -process ejecta. We find that ^{126}Sn , which has several lines in the energy range 415–695 keV and resides close to the second r -process peak, is the most promising isotope, because of its half-life $t_{1/2} = 2.30(14) \times 10^5$ yr being comparable to the ages of recent NSMs. Using a Monte Carlo procedure, we predict that multiple remnants are detectable as individual sources by next-generation γ -ray telescopes which achieve sub-MeV line sensitivities of $\sim 10^{-8}$ – 10^{-6} γ cm $^{-2}$ s $^{-1}$. However, given the unknown locations of the remnants, the most promising search strategy is a systematic survey of the Galactic plane and bulge extending to high Galactic latitudes. Individual known supernova remnants which may be mis-classified NSM remnants could also be targeted, especially those located outside the Galactic plane. Detection of a moderate sample of Galactic NSM remnants would provide important clues to unresolved issues such as the production of actinides in NSMs, properties of merging NS binaries, and even help distinguish them from rare supernovae as current Galactic r -process sources. We also investigate the diffuse flux from longer-lived nuclei (e.g. ^{182}Hf) that could in principle trace the Galactic spatial distribution of NSMs over longer timescales, but find that the detection of the diffuse flux appears challenging even with next-generation telescopes.

Keywords: gamma-ray astronomy, r process

1. INTRODUCTION

Roughly half of the naturally occurring isotopes heavier than the iron group are created through the process of rapid neutron capture (r -process; Burbidge et al. 1957; Cameron 1957; see Cowan et al. 2019 for a recent review). Although the basic physical conditions

needed for the r -process are well understood (e.g. Hoffman et al. 1997), the astrophysical site or sites giving rise to the requisite high neutron flux remains debated. Among the primary candidates are core collapse supernovae (SNe; e.g. Meyer et al. 1992; Takahashi et al. 1994; Woosley et al. 1994) and the coalescence of compact neutron star binaries (Lattimer & Schramm 1974; Symbolist & Schramm 1982; Eichler et al. 1989; Korobkin et al. 2012). For SNe, one can further distinguish the

* NASA Einstein Fellow

neutrino-driven winds from proto-neutron stars (common to most SNe; e.g. Qian & Woosley 1996; Thompson et al. 2001), from the rarer subset of collapse events which give birth to rapidly-spinning highly-magnetized neutron stars (Thompson et al. 2004; Metzger et al. 2007; Winteler et al. 2012; Mösta et al. 2018) or hyper-accreting black holes (Fryer et al. 2006; Siegel et al. 2019).

Our understanding of the r -process advanced dramatically following the discovery of a binary neutron star merger (NSM) through both its gravitational waves (Abbott et al. 2017a) and electromagnetic light (Abbott et al. 2017b). This event, dubbed GW170817, was accompanied by fading visual and infrared emission (e.g. Coulter et al. 2017; Soares-Santos et al. 2017), which was widely interpreted as being powered by the radioactive decay of freshly synthesized r -process nuclei (Li & Paczyński 1998; Metzger et al. 2010; Barnes & Kasen 2013; Tanaka & Hotokezaka 2013). Modeling of the light curve indicates a total r -process ejecta mass of $\approx 0.03\text{--}0.06 M_{\odot}$ (e.g. Drout et al. 2017; Cowperthwaite et al. 2017; Kasen et al. 2017; Villar et al. 2017; Kawaguchi et al. 2018; Wanajo 2018; Wu et al. 2019). The large quantity of ejecta from GW170817 shows that NSMs are major, if not dominant, sources of the Galactic r -process (e.g. Kasen et al. 2017). The mergers of compact binaries comprised of a neutron star (NS) and stellar-mass black hole (BH) can also eject large quantities of neutron-rich r -process material, provided that the BH is rapidly spinning and of sufficiently low mass to tidally disrupt the NS before the latter plunges inside the BH event horizon (e.g. Foucart et al. 2018).

Despite this progress, a few key questions remain open. For instance, it is unclear whether NSMs occur sufficiently promptly following the first generations of star formation in the universe to explain the high r -process abundance in metal-poor halo stars (Snedden et al. 2008) and dwarf galaxies (Ji et al. 2016) (see e.g., van de Voort et al. 2015; Hirai et al. 2015; Shen et al. 2015; Wehmeyer et al. 2015; Côté et al. 2018; Safarzadeh et al. 2019). Studies of Galactic chemical evolution also indicate that the growth in the abundances of Europium relative to α -process elements (which originate mainly from SNe) points to an r -process source which tracks ongoing star formation (Côté et al. 2018; Hotokezaka et al. 2018) instead of the delayed population generally predicted for NSMs (however, see Beniamini & Piran 2019). Separately, it is not clear whether the observed diversity in the abundance patterns of individual Galactic r -process events (Honda et al. 2006; Holmbeck et al. 2018; Ji & Frebel 2018) is an indication of separate production sites (e.g. NS-NS versus NS-BH

mergers versus rare SNe), or diversity within an underlying similar event. While the late-time infrared emission from GW170817 provides evidence for the production of lanthanide elements (atomic number $A \gtrsim 140$; e.g. Chornock et al. 2017; Tanvir et al. 2017; Pian et al. 2017), no strong evidence exists for the production of heavier nuclei near the third r -process peak ($A \gtrsim 195$).

Freshly synthesized r -process elements are radioactive. Gamma-rays (Qian et al. 1998, 1999) or X-rays (Ripley et al. 2014) from decaying r -process nuclei in young supernova (SN) remnants can therefore provide direct evidence of their production. Decay lines from the (non r -process) isotope ^{44}Ti were detected from the SN remnants Cas A (Iyudin et al. 1994; Vink et al. 2001; Renaud et al. 2006; Boggs et al. 2015; Siegert et al. 2015; Grefenstette et al. 2017) and SN 1987A (Grebenev et al. 2012). The biggest challenge to detect r -process elements in SNe remnants is that their expected abundances are many orders of magnitude smaller than lighter nuclei, assuming that the r -process isotopes are produced in equal quantity in all SNe and that the latter are major contributors to the total Galactic r -process abundances. If instead only a small subset of SNe produce the r -process and the per-event yields are higher, then this subset of SNe would have higher line fluxes (but a large number of remnants must then be searched to discover even one r -process source).

Because of their guaranteed larger r -process yields, the remnants of past NSMs in our Galaxy may be more promising γ -ray line sources (Ripley et al. 2014). NSMs occur in the present-day Milky Way (MW) at an estimated rate of $f_{\text{NSM}} \sim 10\text{--}100 \text{ Myr}^{-1}$, a range which is consistent with both studies of the Galactic double neutron star population (e.g. Kim et al. 2010), limits from the LIGO O1/O2 observing runs (The LIGO Scientific Collaboration & the Virgo Collaboration 2018), and constraints based on the r -process yield from GW170817 for total Galactic abundances. The youngest NSM remnant in our Galaxy is therefore of age $\sim 10^4\text{--}10^5 \text{ yr}$, a range fortuitously comparable to the half-lives of several promising r -process isotopes, particularly ^{126}Sn ($t_{1/2} = 2.30(14) \times 10^5 \text{ yr}$; see Table 2).

The kinetic energy of the kilonova ejecta from GW170817 was inferred to be $\sim 10^{51} \text{ erg}$, similar to that of SNe (e.g. Villar et al. 2017). If representative, then the physical size of NSM remnants, following their shock interaction with the interstellar medium (ISM), is similar to those of SN remnants of the same age (Montes et al. 2016). However, since the spatial locations of the NSM remnants (which are far-outnumbered by SN remnants) are not known, detecting their γ -ray line signal may require a creative search strategy, such as a system-

atic search of known remnants which in rare cases might be mis-classified as SNe, or a wide-field survey of the Galactic plane/bulge. Unlike core collapse SNe, which largely take place in the high-density Galactic plane, NSMs can take place with large physical offsets from their birth locations due to NS natal kicks (e.g. [Bloom et al. 1999](#)), in which case their spatial distribution may extend to higher Galactic latitudes.

As with SNe, old NSM remnants of age $\gg 10^6$ yr will eventually have their material mixed into the ISM of the Galactic halo or disk. Decay lines from long-lived nuclei (e.g. ^{182}Hf , with $t_{1/2} = 8.90(9) \times 10^6$ yr) may thus present as a diffuse γ -ray line flux from the Galactic plane, much in the way that ^{26}Al ($t_{1/2} = 7.17(24) \times 10^5$ yr) and ^{60}Fe ($t_{1/2} = 2.62(4) \times 10^6$ yr) are measured in the inner portions of the MW ([Plüschke et al. 2001](#); [Smith 2004](#); [Diehl et al. 2006](#); [Wang et al. 2007](#)).

In this paper, we predict the properties of r -process γ -ray line sources from Galactic NSMs, lay out strategies to detect them, and highlight the scientific returns of such discoveries. We provide the expected number, distances, sky-positions, and angular sizes of sources, as well as their γ -ray line fluxes. For individual remnants, we focus on the lines from ^{126}Sn , given its optimal half-life and large fluxes. Being a nucleus just below the second r -process peak, which does not require particularly neutron-rich ejecta for its creation, ^{126}Sn production in NSMs has the benefit of likely being guaranteed and more robust. While less robustly produced, we also consider decay lines from ^{230}Th ($t_{1/2} = 7.54(3) \times 10^4$ yr), which would probe the presently-unconstrained production of actinides in NSMs. Finally, we estimate the diffuse background from ^{182}Hf , under the assumption that, while individual NSM remnants may have dissolved into the ISM prior to its decay, the angular distribution of ^{182}Hf off the Galactic plane could distinguish different r -process sources.

The line sensitivities of past or existing MeV γ -ray satellites, such as COMPTEL ([Schoenfelder et al. 1993](#)) or INTEGRAL ([Diehl 2013](#)) of $\sim 10^{-5} \gamma \text{ cm}^{-2} \text{ s}^{-1}$, are probably not sufficient to detect r -process lines from NSM remnants. However, proposed next generation balloon or satellite missions could achieve line sensitivities of $\sim 10^{-8}$ – $10^{-6} \gamma \text{ cm}^{-2} \text{ s}^{-1}$ (see a summary in e.g., [Fryer et al. 2019](#)). These include balloon missions such as COSI ([Kierans et al. 2016](#)) and GRAMS ([Aramaki et al. 2019](#)), as well as several satellite missions, e.g., AMEGO ([Moiseev & Team 2018](#)), e-ASTROGAM ([Tavani et al. 2018](#)), ETCC ([Tanimori et al. 2017](#)), HEX-P ([Madsen et al. 2018](#)), and LOX ([Miller et al. 2018](#)).

Rather than addressing the individual prospects of these concepts for NSM remnant science, which will be

heavily dependent on particulars such as the instrument and astrophysical backgrounds, our chief goal with this work is to highlight the key multi-messenger science and to provide concrete predictions to motivate these concept studies.

2. NSM REMNANT DISTRIBUTION

2.1. Spatial Position, Distance, and Age

We model the spatial and age distribution of young (age $\lesssim 50$ Myr) NSM remnants in our Galaxy using the following prescription.

- We assume that the “birth” places of the binary NS systems trace the stellar mass distribution of the MW bulge and disk. We model the latter following [McMillan \(2017\)](#), particularly their eqs. (1)-(3), using the best-fit values from their Table 3 for the MW stellar density. In reality, binary NS systems are formed at essentially the same times and places as the stars themselves. However, neglecting SN kicks, the substantial delay due to the slow process of gravitational wave-inspiral should result in currently-merging binaries tracing the locations of older stars more faithfully than that of current star-formation.
- Neutron stars can receive substantial kicks at birth of up to several hundred km s^{-1} , which affect the locations of NSM events (e.g. [Bloom et al. 1999](#)). From “birth” to merger, we account for this effect by allowing the binary systems to undergo spatial drift from the stellar population, using the observed offset distribution of short-duration gamma-ray bursts (GRB) from their host galaxies from [Fong & Berger \(2013\)](#). We assume the drift directions are isotropically distributed from the birth sites.

Since some short GRBs occur in galaxies with different properties than the spiral-type MW (e.g. elliptical or S0 galaxies), we consider two models for the offset distribution in order to test the sensitivity of our results to our assumptions. Model I uses an offset distribution from Fig. 6 in [Fong & Berger \(2013\)](#) which has been normalized to the effective radius r_e of the host galaxy, taking $r_e = 7.5$ kpc for the MW. Model II instead uses directly the offset distribution in physical units from Fig. 5 in [Fong & Berger \(2013\)](#).

- We consider two values for the current NSM rate in the MW, $f_{\text{NSM}} = 10 \text{ Myr}^{-1}$ and 100 Myr^{-1} . The higher of these rates is near the mean value inferred from the LIGO O1/O2 runs ([The LIGO](#)

Scientific Collaboration & the Virgo Collaboration 2018) while the lower rate represents a “conservative” scenario on the very low end of the allowed rate. We assume that mergers are distributed uniformly in time, which is justified for young merger remnants with ages $\lesssim 100$ Myr much less than the timescale over which the MW star formation rate is currently evolving.

- We perform Monte Carlo sampling over the above temporal and spatial distributions for time spans of 10 Myr for the individual source detection of γ -lines from shorter-lived nuclei ($t_{1/2} \ll 1$ Myr), and 50 Myr for the diffuse lines from longer-lived nuclei ($t_{1/2} \sim 10$ Myr).

The top two rows of Fig. 1 show the probability distributions of the distances (from Earth) of the NSM remnants and their vertical height z off the mid-plane of the MW disk, shown separately for Model I (left panels) and Model II (right panels). The distance distribution in both Models peaks at ~ 10 kpc and smoothly extends to large distances ~ 100 kpc. However, as expected, the width of the distribution in Model I is larger than that in Model II due to the assumed offsets, giving rise to a lower probability of closer remnants in Model I. The distribution of vertical heights is centered about the midplane ($z = 0$) but extending to up to $|z| \sim$ several tens of kpc. The height distribution of Model I is again broader than Model II, but in both cases a significant fraction ~ 20 –40% of the remnants are located within $|z| \lesssim 2$ kpc.

2.2. Physical and Angular Size

Following Cioffi et al. (1988) for the interaction of SN ejecta with the ISM, there are three distinct phases in the evolution of NSM remnants before it merges with the ISM. The initial “free expansion” phase takes place until the swept-up ISM mass equals that of the ejecta, M_{ej} . This occurs after a time

$$t_{\text{sw}} = 69.5 \left(\frac{0.1c}{v_{\text{ej}}} \right) \left(\frac{M_{\text{ej}}}{M_{\odot}} \right)^{1/3} \left(\frac{n}{\text{cm}^{-3}} \right)^{-1/3} \text{ yr}, \quad (1)$$

where v_{ej} is the ejecta velocity and $n \approx \rho/m_p$ is the ISM particle density (here ρ and m_p are the mass density and proton mass, respectively). After a time $t \gtrsim t_{\text{sw}}$, the remnant evolves as an energy-conserving Sedov-Taylor (ST) blast wave, until radiative cooling becomes important after a time

$$t_{\text{PDS}} = t_{\text{sw}} + 1.33 \times 10^4 \left(\frac{E}{10^{51} \text{ ergs}} \right)^{3/14} \left(\frac{n}{\text{cm}^{-3}} \right)^{-4/7} \text{ yr}, \quad (2)$$

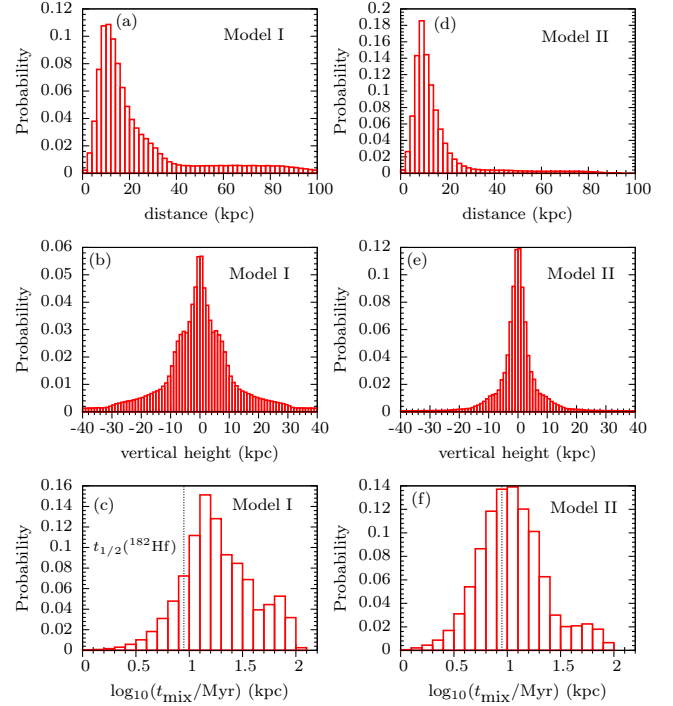


Figure 1. Probability distribution of distances, vertical heights (as measured out of the Galactic plane), and ISM mixing time t_{mix} for a simulated population of Galactic NSM remnants. Results are shown separately for Model I [panels (a)–(c)] and Model II [panels (d)–(f)] for the physical offset of NSMs from the stars (see text). In the bottom panels (c) and (f), the half-life of ^{182}Hf is shown for comparison with a vertical dotted line.

where $E = M_{\text{ej}} v_{\text{ej}}^2/2$ is the ejecta kinetic energy. At times $t \gtrsim t_{\text{PDS}}$, the pressure of the hot interior of the remnant drives the expansion that is further aided by its momentum in a phase known as the “pressure-driven snowplow (PDS)”. Finally, the ejecta merges/mixes with the ISM after a time¹

$$t_{\text{mix}} = 56.84 t_{\text{PDS}} \left(\frac{E}{10^{51} \text{ ergs}} \right)^{5/49} \left(\frac{n}{\text{cm}^{-3}} \right)^{10/49}. \quad (3)$$

¹ At the end of the PDS phase, when most of the interior thermal energy has been depleted due to radiative cooling, the interior pressure becomes negligible. At this point, the remnant enters into the so-called “momentum-conserving snowplow (MCS)” phase, where the expansion is solely driven by the momentum of the remnant. However, as noted by Cioffi et al. (1988), the remnant usually merges with the ISM while still in the PDS or ST phase well before MCS phase is reached. Therefore, we neglect the MCS phase in this work.

Combining the above results, the radius of a NSM remnant of age t is given by

$$\begin{aligned}
 r_{\text{NSM}}(t) &= v_{\text{ej}} t, t \leq t_{\text{sw}} \\
 &= R_{\text{sw}} + \left(\frac{2.026 E (t - t_{\text{sw}})^2}{\rho} \right)^{1/5}, t_{\text{sw}} < t \leq t_{\text{PDS}} \\
 &= R_{\text{PDS}} \left(\frac{4}{3} \frac{t}{t_{\text{PDS}}} - \frac{1}{3} \right)^{3/10}, t_{\text{PDS}} < t \leq t_{\text{mix}} \\
 &= R_{\text{PDS}} \left(\frac{4}{3} \frac{t_{\text{mix}}}{t_{\text{PDS}}} - \frac{1}{3} \right)^{3/10}, t > t_{\text{mix}}, \quad (4)
 \end{aligned}$$

where R_{sw} and R_{PDS} are the values of r_{NSM} at t_{sw} and t_{PDS} , respectively. The expansion velocity of the remnant can then be estimated as $v_{\text{exp}} = dr_{\text{NSM}}/dt$.

To estimate the local value of the ISM density at the location of each NSM remnant, we assume that gas density drops with Galactic radius r and vertical distance z above the MW disk according to the following profile from Miller & Bregman (2013):

$$n(r) = n_0 [1 + (r/R_c)^2 + (z/z_c)^2]^{-3\beta/2} \quad (5)$$

where we take $n_0 = 0.46 \text{ cm}^{-3}$, $R_c = 0.42 \text{ kpc}$, $z_c = 0.26 \text{ kpc}$, and $\beta = 0.71$ from the best-fit values of Miller & Bregman (2013). The angular size α of the remnant diameter in radians is then given by

$$\alpha = \arctan \left(\frac{2r_{\text{NSM}}}{d} \right), \quad (6)$$

where d is the remnant distance.

The bottom panels of Fig. 1 show the distribution of t_{mix} for all of the NSM remnants in our Monte Carlo sample, assuming ejecta parameters $E = 10^{51} \text{ erg}$ and $M_{\text{ej}} = 0.04 M_{\odot}$, motivated by observations of GW170817. A minimum value of $t_{\text{mix}} \sim 1 \text{ Myr}$ is reached near the densest regions in the Galactic Center (GC), but the distribution peaks at $\sim 10 - 15 \text{ Myr}$ and extends to larger values $\sim 100 \text{ Myr}$. As the mixing times are much longer than the half-lives of several of the isotopes of greatest interest (e.g. ^{126}Sn , ^{230}Th), these γ -ray lines should still be found as singularly associated with individual NSM remnant (Sec. 3). By contrast, the mixing time can be comparable to the half-life of ^{182}Hf (shown as a vertical dashed line in Fig. 1), indicating that this isotope might be substantially mixed with the ISM, in which case it would instead form a more diffuse γ -ray background (Sec. 4).

3. INDIVIDUAL REMNANTS

There are only 22 known X- and γ -ray emitting radioactive r -process nuclei with half-lives ($t_{1/2}$) in the range $10^2 - 10^8$ years. Table 2 in the Appendix lists

their decay sequences, half-lives, and the major X- and γ -ray line energies and intensities (probability of emitting a γ per decay). Figure 7 in the Appendix shows an example of the X-ray/ γ -ray line spectrum of a remnant of age $\approx 5 \times 10^4 \text{ yr}$ and distance of 9 kpc, similar to those of the youngest Galactic NSM remnants.

Among these isotopes, ^{126}Sn , which resides close to the second r -process peak, with $t_{1/2} = 2.3 \times 10^5 \text{ yr}$, is the most promising candidate for NSM remnant γ -ray searches. First, the decay sequence of $^{126}\text{Sn} \rightarrow ^{126}\text{Sb} \rightarrow ^{126}\text{Te}$ produces a few strong lines with energy (intensity) of 414.7 keV (98%), 666.3 keV (100%), 695.0 keV (97%) (Orth et al. 1971; Bargholtz et al. 1975; Smith et al. 1976)² Second, the production of nuclei near the second peak, like ^{126}Sn , is almost guaranteed in every NSM. Motivated thus, we evaluate the detection prospect of ^{126}Sn decay γ -rays in Sec. 3.1 and then discuss the possibility of co-detecting other lines from the actinide decay in Sec. 3.2.

3.1. ^{126}Sn Individual Sources

We assume that each NSM produces an ejecta mass $M_{\text{ej}} = 0.04 M_{\odot}$, consistent with the inferred production yield of GW170817, and contains a distribution of r -process nuclei following the Solar r abundances in the mass range $A = 90 - 205$ taken from Sneden et al. (2008)³. This gives a corresponding number fraction per nucleon, or abundance, of ^{126}Sn at production, $Y_0 = 1.7 \times 10^{-4}$.

We then generate 10^3 and 10^4 realizations for the assumed NSM frequency $f_{\text{NSM}} = 100 \text{ Myr}^{-1}$ and 10 Myr^{-1} , respectively, following the method described in Sec. 2 for both Model I and II. For each remnant, we calculate the photon number flux $F(d, t)$ with an intensity $I_g = 100\%$, which corresponds to the intensity of the strongest lines at 666.3 keV from the decay of

² Note that the decay of ^{126}Sn populates the first excited isomeric state of ^{126}Sb ($J^\pi = 5^+$) before reaching its ground state ($J^\pi = 8^-$). This isomeric state has a branching ratio of 86(4)% by β -decay to ^{126}Te , and 14(4)% by isomeric-transition to the ground state of ^{126}Sb (Orth et al. 1971), which further β -decays to ^{126}Te . Therefore, the decay line intensities from ^{126}Sb are a linear-superposition of these two sub-channels. For example, a 720.7 keV line has a 53.80(24)% intensity (Bargholtz et al. 1975) via the latter channel but will not be produced via the former, which results in a total intensity of only $\approx 7\%$.

³ The Solar r abundances in Sneden et al. (2008) are given for elements with charge number $Z \geq 69$. However, we do not include those between $69 \leq A \leq 89$ because their solar r abundances may have received large contribution from other sites like core collapse SNe. Moreover, the observed metal-poor star abundances suggests that nuclei around $A \sim 70$ are likely not co-produced by NSMs (Cowan et al. 2005).

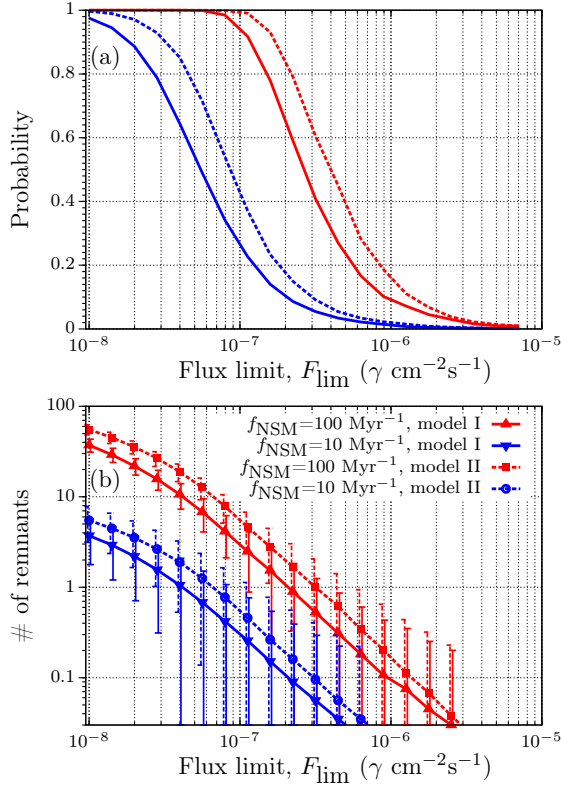


Figure 2. Panel (a): Probability of the existence of at least one NSM remnant with a ^{126}Sn γ -ray line flux exceeding a given flux limit, F_{lim} . We show separately the results for two assumptions for the spatial offset of NSMs (Model I and Model II), and for two merger rates, $f_{\text{NSM}} = 10 \text{ Myr}^{-1}$ and 100 Myr^{-1} . Panel (b): Number of remnants with γ -ray line flux $\geq F_{\text{lim}}$ as a function of F_{lim} for the same scenarios as in the top panel. Thick curves show the detected number averaged over all realizations, while vertical error bars show the $\pm 1\sigma$ sample variance.

^{126}Sn :

$$F(d, t) = \frac{M_{\text{ej}} Y_0 I_g}{4\pi d^2 m_u \tau_0} e^{-t/\tau_0}, \quad (7)$$

where m_u is the atomic mass unit and $\tau_0 = 2.3 \times 10^5 \text{ yr} / \ln(2)$ is the lifetime of ^{126}Sn . For a given threshold flux limit F_{lim} , we then calculate the number of NSM remnants having $F(d, t) > F_{\text{lim}}$ for all realizations, separately in each model and for both values of f_{NSM} .

Figure 2 shows the probability of having *at least one* remnant (top panel), as well as the expected number of remnants (bottom panel), for which the ^{126}Sn line flux exceeds a given limiting value F_{lim} . Our results do not depend sensitively on the chosen model of the remnant offset distribution. Compared to Model I, Model II yields a slightly higher probability because its predicted smaller offset distribution leads to mergers being on average closer (Fig. 1).

The detection probability does, however, depend sensitively on the assumed NSM rate, f_{NSM} . For the value $f_{\text{NSM}} = 100 \text{ Myr}^{-1}$ in the middle of the range allowed by the LIGO discovery of GW170817, we find that ~ 1 – 5 remnants have line fluxes above $F_{\text{lim}} \sim 10^{-7} \gamma \text{ cm}^{-2} \text{ s}^{-1}$, with a $\gtrsim 90\%$ probability of at least one remnant above this threshold. For a lower detection threshold $F_{\text{lim}} \sim 10^{-8} \gamma \text{ cm}^{-2} \text{ s}^{-1}$, the prospects are obviously better. Even for the most conservative merger rate $f_{\text{NSM}} = 10 \text{ Myr}^{-1}$, the probability of having more than one merger remnant with line flux above F_{lim} is as large as 96%. For the high merger rate $f_{\text{NSM}} = 100 \text{ Myr}^{-1}$, there should exist $\gtrsim 30$ NSM remnants above $10^{-8} \gamma \text{ cm}^{-2} \text{ s}^{-1}$.

Figure 3 further shows distribution of distances, ages, Galactic latitudes, longitudes, angular sizes, vertical heights, expansion velocities v_{exp} , and γ -ray line flux $F(d, t)$, for all remnants satisfying $F(d, t) > F_{\text{lim}} = 10^{-8} \gamma \text{ cm}^{-2} \text{ s}^{-1}$ (for Model I with $f_{\text{NSM}} = 100 \text{ Myr}^{-1}$). The detectable remnant population are mostly younger than 1 Myr and located at characteristic distances of $\sim 9 \text{ kpc}$. Most have angular sizes of $\sim 2^\circ$ and are within $\sim \pm 5 \text{ kpc}$ of Galactic plane. Most of the remnants have low expansion velocities $v_{\text{exp}} < 3 \times 10^3 \text{ km s}^{-1}$, indicating narrow predicted γ -ray line widths (Sec. 5.2).

Interestingly, roughly 40% of the remnants reside within $\pm 20^\circ$ from the GC. Furthermore, $\sim 4\%$ and 17% of the NSM remnants are located inside \sim the Galactic bulge defined by a sphere with a radius of 2 kpc and the galactic disk defined by a typical scale height of 1 kpc, respectively. As we discuss in Sect. 5, this motivates a survey strategy focused on the Galactic plane and bulge. Figure 4 shows one realization (from Model I, with $f_{\text{NSM}} = 100 \text{ Myr}^{-1}$) of the sky map of spatial positions and γ -ray fluxes of remnants obeying $F(d, t) > F_{\text{lim}} = 10^{-8} \gamma \text{ cm}^{-2} \text{ s}^{-1}$. The distances and vertical heights of the detectable population of NSM remnants are usefully contrasted with those of known Galactic SN remnants, shown in Fig. 8 in the Appendix.

3.2. Actinides as Secondary Tracers

As listed in Table 2, most of the γ -ray emitting nuclei with half-lives in the range $100 \text{ yr} \leq t_{1/2} \leq 100 \text{ Myr}$ are actinides with mass number $226 \leq A \leq 250$. Among these, the most promising candidate for an individual remnant search together with ^{126}Sn (i.e. with a comparable half-life) is ^{230}Th ($t_{1/2} = 7.54(3) \times 10^4 \text{ yr}$). ^{230}Th decays via a long decay chain ending at ^{206}Pb and produces a couple of strong γ -ray lines at sub-MeV energies, e.g., 351.9 keV (35.6%) and 609.3 keV (45.5%). Despite the somewhat weaker intensity of these lines, due to its

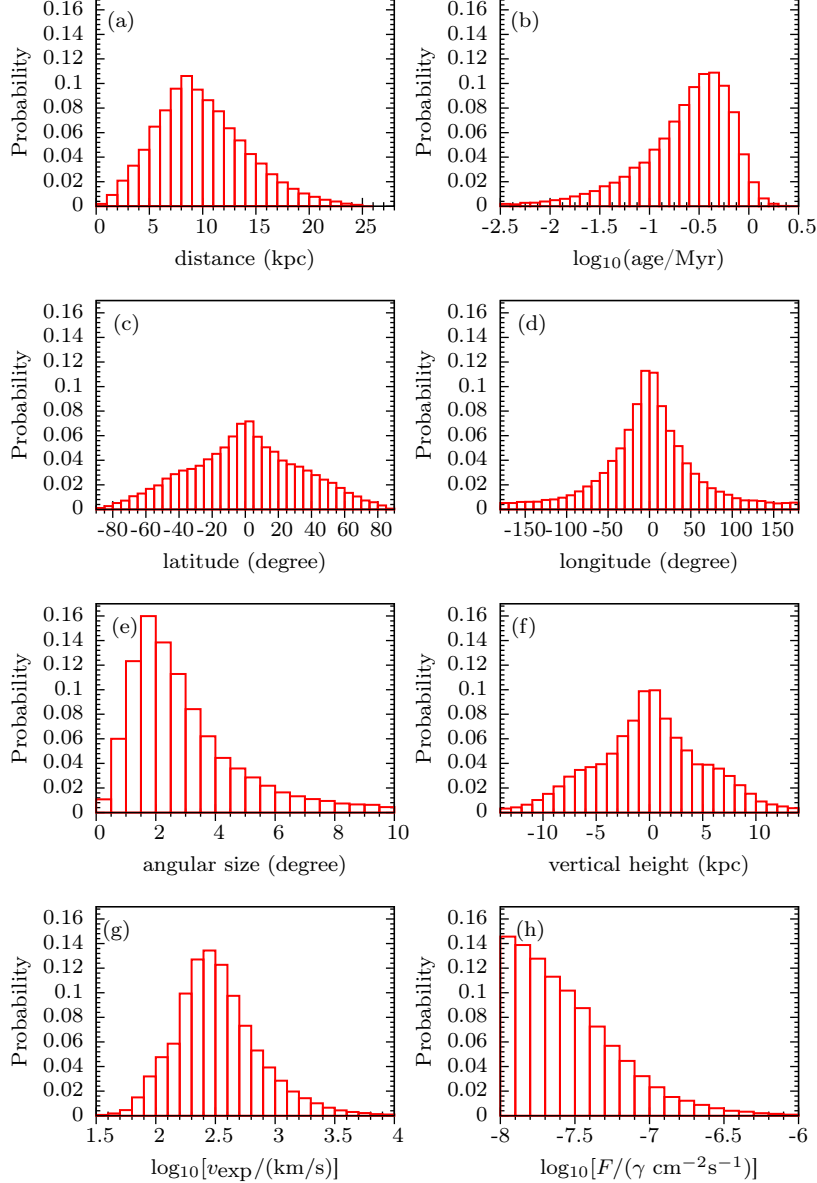


Figure 3. Probability distributions of several key properties of NSM remnants with ^{126}Sn γ -ray line fluxes $F \geq 10^{-8} \gamma \text{ cm}^{-2} \text{ s}^{-1}$. Properties shown include distance, age, latitude, longitude (in the Galactic coordinate), angular size, vertical height above the MW disk, remnant expansion velocity v_{exp} , and line flux $F(d, t)$ at 666.3 keV. We use Model I for the NSM spatial offsets and assume a Galactic NSM rate of $f_{\text{NSM}} = 100 \text{ Myr}^{-1}$. For all remnants, we have assumed an r -process ejecta mass $M_{\text{ej}} = 0.04 M_{\odot}$ with $Y(^{126}\text{Sn}) = 1.7 \times 10^{-4}$.

shorter half-life, ^{230}Th can generate comparable γ -ray flux as ^{126}Sn for an otherwise similar abundance.

Unfortunately, the production of actinides in NSMs is uncertain because it requires highly neutron-rich conditions (very low electron fraction), which may not characterize the bulk of the NSM ejecta. Nevertheless, one can still estimate the actinide abundance empirically if one assumes that NSMs must on average produce the measured solar- r thorium and europium abundances. In this case, the number fraction of individual actinide nuclei in

the merger ejecta is roughly given by $Y_{\text{act}} \simeq 3.6 \times 10^{-6}$, under the following assumptions: (i) NSMs occur with a uniform frequency over the MW's history $\sim 13 \text{ Gyr}$; (ii) Only actinides between $226 \leq A \leq 250$ produced by NSMs contribute to the solar system ^{232}Th abundance, i.e., nuclei heavier than $A = 250$ mostly fission away during and after the r -process (Giuliani et al. 2019). (iii) Each NSM produces uniform actinide abundances across the above mass range. On the other hand, abundance measurements from metal-poor stars (those polluted by

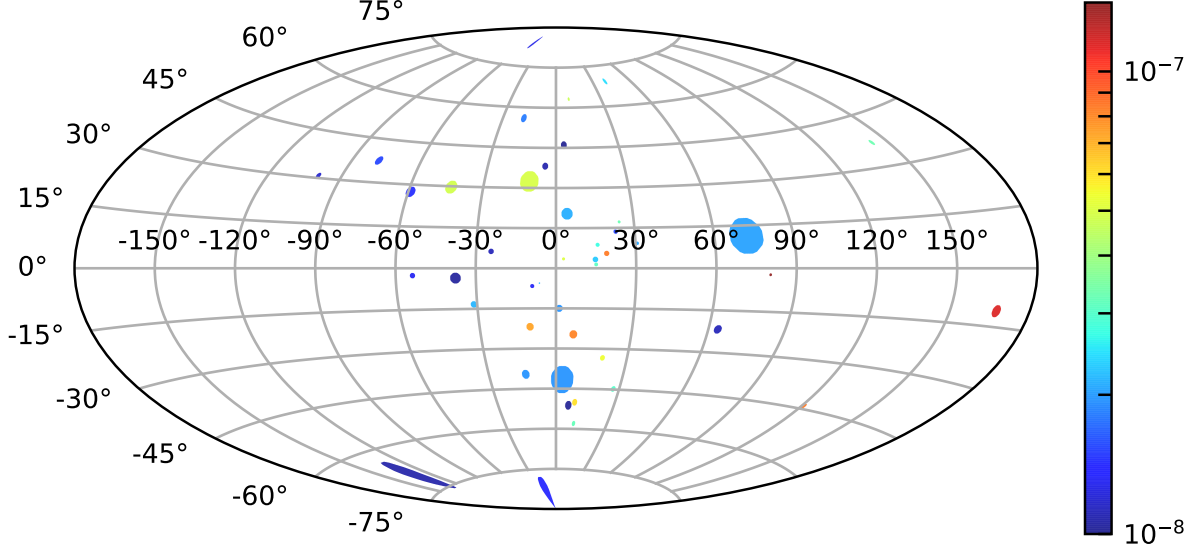


Figure 4. Example realization of the sky map of individual NSM remnant γ -ray sources with line fluxes $F > F_{\text{lim}} = 10^{-8} \gamma \text{ cm}^{-2} \text{ s}^{-1}$ for the same scenario in Fig. 3. The circular/elliptical shaded areas represent the angular sizes of the remnants and the colors represent the emitted 666.3 keV line fluxes in units of $\gamma \text{ cm}^{-2} \text{ s}^{-1}$, indicated on the legend. The center of the plot marks the direction of the GC.

just a single, or at most a few, r -process events) indicate that the intrinsic Th production yields may vary by a factor of ~ 3 from event to event (Holmbeck et al. 2018; Ji & Frebel 2018). Furthermore, theoretical predictions of the actinide abundances based on nuclear reaction network calculations can vary up to a factor of ~ 10 , depending on the assumed nuclear mass models and the beta-decay half-lives (see e.g., Holmbeck et al. 2019; Eichler et al. 2019).

Due to these uncertainties, we assess the detection prospects of actinides in NSM remnants as a function of the actinide abundance. We focus on the ^{230}Th decay line at 609.3 keV with $I_g = 45.5\%$. Since ^{230}Th is also the daughter of ^{234}U (half-life $t_{1/2} = 2.46 \times 10^5 \text{ yr}$), together they produce a photon number flux:

$$\tilde{F}(d, t) = \frac{M_{\text{ej}} Y_{\text{act}} I_g}{4\pi d^2 m_u} \times \left[\frac{1}{\tau_a} e^{-t/\tau_a} + \frac{1}{\tau_a - \tau_b} (e^{-t/\tau_a} - e^{-t/\tau_b}) \right], \quad (8)$$

where Y_{act} is the number fraction of both ^{230}Th and ^{234}U , and τ_a and τ_b are the lifetimes of ^{230}Th and ^{234}U , respectively.

Fig. 5 shows the fraction of NSM remnants, considered among the population with ^{126}Sn γ -ray fluxes $[F(d, t)]$ above the assumed detection limit $F_{\text{lim}} = 10^{-8} \gamma \text{ cm}^{-2} \text{ s}^{-1}$, which also produce ^{230}Th fluxes $[\tilde{F}(d, t)]$ above the same value F_{lim} , as a function of Y_{act} . We show separately the results for Model I and II, both assuming $f_{\text{NSM}} = 100 \text{ Myr}^{-1}$. The fraction

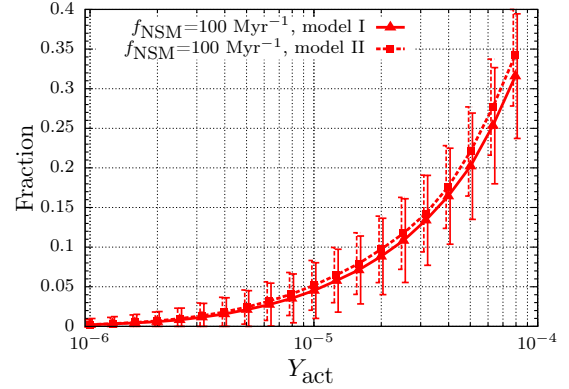


Figure 5. Fraction of NSM remnants that produce γ -line fluxes larger than $F_{\text{lim}} = 10^{-8} \gamma \text{ cm}^{-2} \text{ s}^{-1}$ from both the decay of ^{126}Sn and ^{230}Th as a function of the actinide abundance at production, Y_{act} , normalized to all remnants with ^{126}Sn fluxes exceeding the same F_{lim} . We show results separately for Model I and II, and in each case assume a Galactic merger rate $f_{\text{NSM}} = 100 \text{ Myr}^{-1}$.

satisfying both $F > F_{\text{lim}}$ and $\tilde{F} > F_{\text{lim}}$ grows roughly linearly with Y_{act} within this abundance range. Therefore, by measuring this fraction (e.g. the number of NSM remnants which are detectable just by their ^{126}Sn lines to those also detectable through their ^{230}Th lines), one could in principle determine the average actinide production yield, Y_{act} . By exploring the distributions of line fluxes (in conjunction with independent estimates of the source age), it would also be possible to infer the diversity in actinide yields and compare to that inferred

from the abundances of metal-poor stars. For instance, given the large predicted quantity of low electron fraction tidal-tail ejecta in some NS-BH mergers compared to that in NS-NS mergers (e.g. Foucart et al. 2018), a particularly actinide-rich remnant might implicate a NS-BH merger event.

4. DIFFUSE EMISSION

In addition to the individual γ -ray sources discussed in the previous section, there exists a diffuse γ -ray line background from longer-lived nuclei with lifetimes $\gtrsim 1$ Myr comparable to or exceeding the mixing time of the remnants with the Galaxy ISM (bottom panels of Fig. 1). Among the longer-lived nuclei, ^{182}Hf ($t_{1/2}=8.9$ Myr) is arguably the most promising candidate because of its relatively strong line at ~ 1.1 MeV ($I_g = 35\%$).

Taking an abundance of $Y(^{182}\text{Hf}) = 7 \times 10^{-6}$ in the NSM ejecta, again scaled from the solar r -process abundances, we calculate the diffuse flux (integrated over all mergers over a 50 Myr time span), as well as the flux per solid angle at different sky locations. We consider two cases: (1) Model I with $f_{\text{NSM}} = 100 \text{ Myr}^{-1}$; (2) an otherwise similar case but which assumes zero physical offset, i.e., that the NSMs directly trace the distribution of Galactic stellar mass.⁴

For the first (second) case, we find a total diffuse ^{182}Hf flux integrated over the entire sky of $\sim 2 \times 10^{-8} (1 \times 10^{-7}) \text{ } \gamma \text{ cm}^{-2} \text{ s}^{-1}$. Fig. 6 shows, for one realization in each case, the flux distribution as a function of solid angle in Galactic coordinates. For Model I (top panel), which includes spatial offsets of the NSMs from the stars, the diffuse flux extends to large galactic latitudes but remains peaked around the GC. For the zero-offset case (bottom panel), the diffuse fluxes instead mostly traces the Galactic plane. Unfortunately, in either case the diffuse r -process flux is sufficiently low $\sim 10^{-10} \text{ } \gamma \text{ cm}^{-2} \text{ s}^{-1} \text{ deg}^{-2}$ that its detection appears beyond the capabilities of even next-generation γ -ray facilities.

Naively, guidance as to the Galactic distribution of r -process lines could come from observations of ^{26}Al , which has previously been detected through its 1.8 MeV decay line (Plüschke et al. 2001; Diehl et al. 2006). High energy resolution γ -ray spectroscopy reveals that ^{26}Al

rotates in the same general sense as the Galaxy but has large velocities in comparison to other components of the ISM. Krause et al. (2015) explore the hypothesis that this behavior can be explained from the kinematics of “superbubbles” created by the correlated SN explosions mixing the ejecta into the hot phase of the ISM. By contrast, the delay time of NSM should result in uncorrelated activity and therefore the kinematics could be substantially different. The eventual measurement of such spatial and kinematic properties could therefore help distinguish NSMs from SN sources of the r -process.

5. SEARCH STRATEGIES

This section addresses general strategies to discover or confirm Galactic r -process γ -ray line sources.

5.1. Individual Known Remnants

One strategy to discover r -process line emission is to search individual known core-collapse SN remnants. Although ordinary SNe are no longer considered promising sources for the heaviest r -process elements, they might in some cases produce lighter r -process nuclei extending up to the second peak. Furthermore, certain rare classes of SNe (e.g. those which produce strongly-magnetized neutron stars; e.g. Thompson et al. 2004; Metzger et al. 2007; Winteler et al. 2012; Mösta et al. 2018) might eject sufficiently neutron-rich material to create even the heavier r -process nuclei, similar to a NSM. Finally, one cannot exclude the possibility that a small number of suspected “SN remnants” are in fact NSM remnants, as the two could appear similar at late times in the remnant evolution.

We compute the expected ^{126}Sn decay line fluxes from all known SN remnants in the catalog of Ferrand & Safi-Harb (2012)⁵, normalized to a scenario in which each contains an r -process mass of $M_r \sim 0.01 M_\odot$ (i.e. a ^{126}Sn mass of $\sim 2.14 \times 10^{-4} M_\odot$ assuming solar r abundances). As compiled in Table 1, we find 18 remnants that, depending on their uncertain distances and ages, could produce 666.3 keV line fluxes larger than $10^{-6} (M_r/10^{-2} M_\odot) \text{ } \gamma \text{ cm}^{-2} \text{ s}^{-1}$. Particularly interesting are those cases located outside the Galactic plane and without clear evidence for a NS compact object, and which therefore could in principle be NSMs masquerading as SN remnants. In addition, remnants without clear evidence of X-ray lines associated with α -elements (O, Mg, Si, S) or Fe (e.g. as formed in SNe but not NSMs) may be worth targeting.

⁴ The latter model may provide a reasonable approximation for the spatial distribution of r -process production in scenarios invoking rare types of SNe, such as the birth of rapidly-spinning magnetars (Thompson et al. 2004; Winteler et al. 2012) or collapsars (Siegel et al. 2019), as major r -process sources. However, in principle the remnants from SNe should more tightly trace the locations of current star formation.

⁵ Updated data in <http://www.physics.umanitoba.ca/snr/SNRcat/>

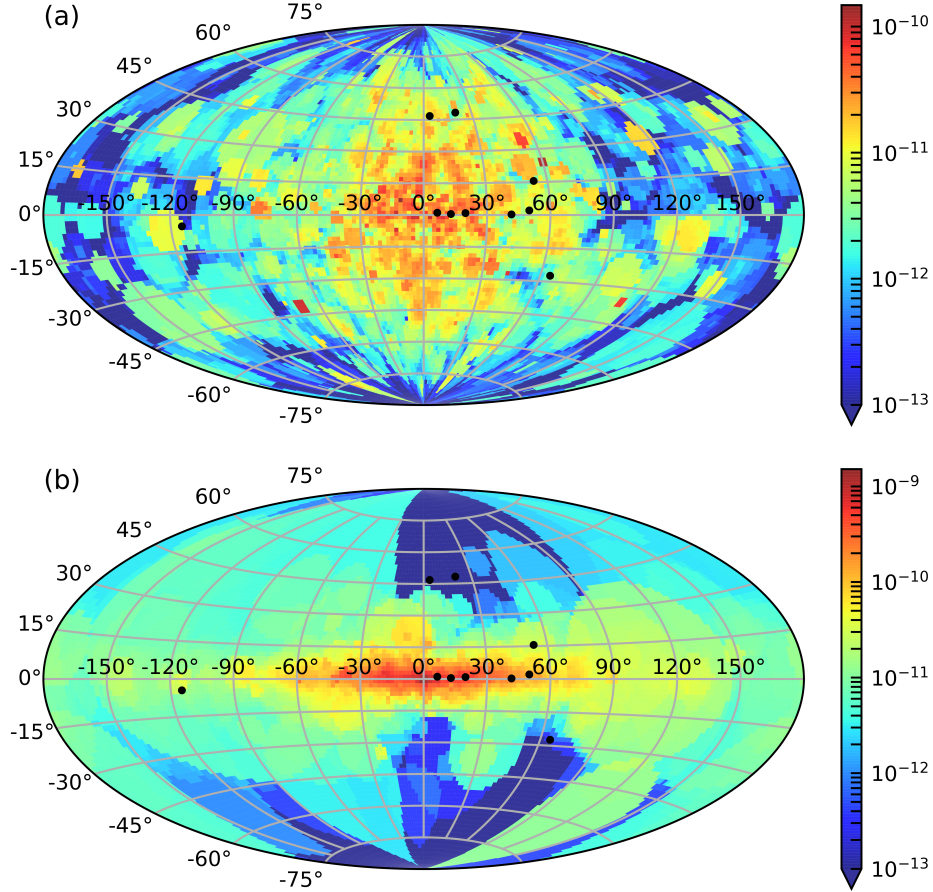


Figure 6. Example realizations of the diffuse flux from the 1.121 MeV decay line of ^{182}Hf per unit solid angle (in units of $\gamma \text{ cm}^{-2} \text{ s}^{-1} \text{ deg}^{-2}$), shown separately for (a) Model I with frequency of $f_{\text{NSM}} = 100$ Myr, and (b) with the same frequency but assuming that mergers follow the distribution of stars, i.e., no spatial offset due to NS kicks. Black dots show the locations of known double neutron star systems (Lorimer 2008), which are primarily concentrated in the Galactic plane.

Also of potential interest are remnants containing magnetar compact objects, as these highly-magnetized neutron stars could be formed in MHD supernovae (e.g. Winteler et al. 2012; Mösta et al. 2018) with an appreciably different proto-neutron star wind (e.g. Thompson et al. 2004; Metzger et al. 2007; Vlasov et al. 2017), which could make them more promising r -process sources than SNe producing less-magnetized NSs. Moreover, some magnetars may in fact be born from the NSM (Metzger et al. 2008; Xue et al. 2019), although the fraction is likely to be only a few percent (e.g., Margalit & Metzger 2019). We calculated the ^{126}Sn decay line fluxes from known magnetars listed in Olausen & Kaspi (2014)⁶ using the estimated distances and their characteristic ages. We find that in all cases the line fluxes of magnetar remnants are smaller than $10^{-6} \gamma \text{ cm}^{-2} \text{ s}^{-1}$.

⁶ Data taken from <http://www.physics.mcgill.ca/~pulsar/magnetar/main.html>

Among these, SGR 0501+4516 has a possible association with the SN remnant HB9. However, its predicted flux is only $\sim 4 \times 10^{-7} \gamma \text{ cm}^{-2} \text{ s}^{-1}$, which is smaller than that from the HB9, due to the estimated distance of ~ 2 kpc for the magnetar SGR 0501+4516, versus the smaller lower bound on the distance range 0.4–1.2 kpc for the HB9 remnant (Table 1).

A complete list of the SN remnants/magnetars and their predicted fluxes can be downloaded from Wu et al. (2019).

5.2. Survey of Plane and Bulge

The most recent Galactic NSMs are likely not associated with known SN remnants. While many planned future γ -ray satellites have all-sky monitors that will image the entire sky, for pointed instruments the discovery of NSM remnants may therefore require a systematic search of the Galactic plane or bulge for the r -process γ -ray line emission. To have a high probability of detecting at least a single remnant, the search should reach a

sensitivity of $\lesssim 3 \times 10^{-8} \gamma \text{ cm}^{-2} \text{ s}^{-1}$ (Fig. 2). The predicted angular sizes of the remnants are several degrees (Fig. 3), comparable to the angular resolution of Compton γ -ray telescopes. The search should ideally extend to Galactic latitudes $\pm 20^\circ$ (Fig. 3). A sizable fraction ($\sim 30\%$) of the detectable merger remnants come from the direction of the Galactic bulge. The astrophysical background in this region is greater, but the ability to integrate longer on this single region might overcome some of this deficiency.

Although the most recent Galactic NSM remnant is likely of age $\gtrsim 10^4 - 10^5$ yr, it could be substantially younger. The probability of a NSM of age $\lesssim 1$ kyr is $\lesssim 10\%$, but such a remnant (or an equally young r -process enriched SN remnant) would have substantially higher γ -ray luminosity than predicted for ^{126}Sn and ^{230}Th , due to enhanced contributions from shorter-lived actinide nuclei (e.g. those given in the first few rows in Table 2).

The old NSM remnants of interest will be expanding into the ISM at velocities of $\lesssim 3000 \text{ km s}^{-1}$ (Fig. 3). This implies that the Doppler broadening or offset of the γ -ray lines will be relatively modest, at the level of $\Delta E/E \lesssim v_{\text{exp}}/c \lesssim 1\%$ or less (if the r -process ejecta is concentrated in the low velocity center of the remnant). Similar or smaller offsets in the energy of the line center are expected from the center-of-mass motion of the remnants due to the rotational velocity of the MW or their motion relative to the disk due to natal supernova kicks. A γ -ray telescope with percent- or sub-percent level energy resolution would therefore be needed to resolve these line features.

5.3. X-ray Confirmation of Candidates

In addition to γ -ray lines from distinct isotopes (e.g. ^{230}Th), another way to confirm r -process remnants is with follow-up observations by X-ray satellites (Ripley et al. 2014). Our most promising isotope, ^{126}Sn , contains X-ray L and K lines centered around 4 keV and 28 keV with summed intensities of $\sim 10\%$ and 30% , respectively. For sources with 666.3 keV γ -ray line flux exceeding $\sim 2 \times 10^{-7} \gamma \text{ cm}^{-2} \text{ s}^{-1}$, the resulting predicted X-ray line strength at ~ 4 keV and 28 keV would be $\gtrsim 10^{-16} \text{ erg cm}^{-2} \text{ s}^{-1}$ and $\gtrsim 2 \times 10^{-15} \text{ erg cm}^{-2} \text{ s}^{-1}$. Although unlikely to be detectable with current X-ray telescopes (e.g. XMM, NuSTAR, or NICER), our preliminary estimation indicates that they may possibly be within the reach of future high-sensitivity missions such as eXTP (Zhang et al. 2016), STROBE-X (Ray et al. 2018), and Athena (Nandra et al. 2013) for the ~ 4 keV line and HEX-P (Madsen et al. 2018) for the ~ 28 keV line.

5.4. Merger remnants or SN remnants?

The detection of the decay γ -ray or X-ray lines from the r -process nucleus ^{126}Sn or actinides does not directly imply that the emitting source is a NSM remnant. As discussed before, it may in fact belong to a rare type of SNe. Below we propose several ways to differentiate the two scenarios.

First, although Fig. 3 shows that the NSM remnants preferentially sit toward the direction of the GC, their distributions in Galactic latitude and vertical height show striking differences when compared with those from known SN remnants (see Fig. 8). Due to the offsets from their birth sites, most of the merger remnants ($\sim 80\%$) have vertical heights $|z| \gtrsim 1$ kpc, while nearly all SN remnants are located within the MW disk with $|z| \lesssim 0.2$ kpc. Thus, for merger remnants, only $\sim 15\%$ are expected to be within a latitude of $\pm 5^\circ$, while one expects $\gtrsim 90\%$ of SN remnants to be within this latitude (see also Fig. 6 which illustrates such difference in terms of diffuse sources). Consequently, if a detected remnant has large latitude or vertical distance from the disk, it can be identified unambiguously as a remnant associated with a NSM. This fact also highlights again that if future missions can detect ^{126}Sn decay γ -rays lines from $\gtrsim 10$ remnants (see Fig. 2), it will likely be able to tell us whether NSMs or rare SNe are the dominant sites of r -process nucleosynthesis in the recent history of the MW.

For remnants found to be within the MW disk, if they happen to be nearby, $\lesssim 2$ kpc, the 1.8 MeV γ -ray line flux from the decay of ^{26}Al can be larger than $\sim 10^{-7} \gamma \text{ cm}^{-2} \text{ s}^{-1}$, for an assumed typical yield of ^{26}Al mass of $\sim 5 \times 10^{-5} M_\odot$ from a SN (e.g., Limongi & Chieffi (2006); Tur et al. (2010); Sieverding et al. (2018)). As the production of ^{26}Al in NSM should be negligible, a co-detection of ^{26}Al decay line, together with the lines from ^{126}Sn can, therefore, be used to indicate whether a close-by remnant is resulting from NSM or SN. Likewise, potential 1.17 & 1.33 MeV γ lines from $^{60}\text{Fe} \rightarrow ^{60}\text{Co} \rightarrow ^{60}\text{Ni}$, or the ~ 3.3 keV (5.4 keV) X-ray lines from the decay of ^{41}Ca (^{53}Mn), if identified, will similarly indicate that the emitting source is not a NSM remnant. Moreover, X-ray signature at 0.5–10 keV due to the presence of α -elements and/or the iron group in a young remnant (Vink 2012) before entering the Sedov-Taylor phase will certainly rule out the remnant being associated with a NSM.

6. DISCUSSIONS AND CONCLUSIONS

Detecting r -process γ -ray line emission from extremely young extragalactic NSMs (e.g. those discovered by LIGO) is likely to be challenging for the

Table 1. Ages, distances, and predicted ^{126}Sn γ -ray line fluxes at 666.3 keV for nearby SN remnants for which the latter range exceeds $10^{-6} \gamma \text{ cm}^{-2} \text{ s}^{-1}$. We assume an ejecta mass $M_{\text{ej}} = 0.01 M_{\odot}$ and $Y(^{126}\text{Sn}) = 1.7 \times 10^{-4}$. The final column indicates the possible association of a compact object (P, M, CCO, PWN denote “pulsar”, “magnetar”, “central compact object”, and “pulsar wind nebula”, respectively).

Source	Age (10^3 yr)	Distance (kpc)	Line Flux ($10^{-6} \gamma \text{ cm}^{-2} \text{ s}^{-1}$)	Compact Object or PWN?
Lupus Loop	15–31	0.15–0.5	5.80–67.60	P?
Vela	9–27	0.25–0.3	16.30–24.78	P
Antlia	$(1-6) \times 10^3$	0.06–0.34	0–21.75	P? CCO?
HB9	4–7	0.4–1.2	1.08–9.83	M?
Vela Jr	2.4–5.1	0.5–1.0	1.57–6.32	CCO? P?
3FGL J2014.4+3606	11–12	0.5–4	0.10–6.16	–
Cygnus Loop	10–20	0.576–1	1.50–4.65	PWN?
Monoceros Loop	30–150	0.6–1.98	0.26–4.04	?
IC443	3–30	0.7–2	0.36–3.22	?
2FGL J2333.3+6237	7.7	0.7	3.17	P?
HB21	4.8–15	0.8–2.1	0.34–2.45	–
G65.3+5.7	20	0.8	2.34	P?
RX J1713.7–3946	1–2.1	1	1.58–1.59	CCO?
DA 495	7–155	1–3.6	0.08–1.56	PWN?
G107.5–01.5	3–6	1.1	1.29–1.30	–
CTA 1	13	1.1–1.7	0.53–1.26	P
S147 Sh2–240	26–34	1.1–1.5	0.64–1.22	P
R5	20–30	1.15	1.10–1.13	–

foreseeable future given their large distances (e.g. [Hotokezaka et al. 2016](#); [Li 2019](#); [Korobkin et al. 2019](#)). Motivated by earlier work ([Qian et al. 1998, 1999](#); [Ripley et al. 2014](#)) on γ -ray and X-ray line emission from the MW r -process sources, as well as the measured rate of NSMs by LIGO/Virgo Collaboration and the r -process yield inferred from GW170817, we have shown that the detection of ^{126}Sn decay is possible from the most recent NSM remnants in our Galaxy for future MeV γ -ray telescopes which reach photon line flux sensitivities of $\lesssim 10^{-7} - 10^{-6} \gamma \text{ cm}^{-2} \text{ s}^{-1}$. Furthermore, the co-detection of decay lines from ^{230}Th in such remnants would constrain the uncertain yield of actinides, a question which remains open in spite of the kilonova detection from GW170817 ([Wanajo 2018](#); [Zhu et al. 2018](#); [Wu et al. 2019](#)). Detection of the diffuse line background from ^{182}Hf could in principle map out the spatial distribution of r -process sources over the past $\lesssim 10$ Myr, allowing for another test of NSM versus SN origin based on the vertical extent of this emission above the Galactic plane. However, the low level of the diffuse flux $\lesssim 10^{-10} \gamma \text{ cm}^{-2} \text{ s}^{-1} \text{ deg}^{-2}$ will be a challenging target even for next generation γ -ray telescopes.

Arguably the biggest challenge in detecting γ -ray emission from NSM remnants is finding their locations in the first place. A wide-field search would naturally be conducted for future planned all-sky monitors, such as

AMEGO, COSI, e-ASTROGAM, GRAMS, and LOX. However, for pointed telescopes with narrower fields of view, the remnant population would most easily be discovered via a systematic search of the Galactic plane prioritized toward the GC/bulge, as we predict most detectable remnants to reside within $\pm 20^\circ$ of the GC. Moreover, since a very small fraction of nearby “SN remnants” could in fact be NSM remnants, or arising from rare classes of explosions that synthesize heavy r -process elements (particularly those supernovae creating magnetars), pointed searches for ^{126}Sn γ -lines from these remnants are promising initial test targets for next-generation γ -ray detectors. We also note that although the line flux integrated over a large angular area can be much higher than the fluxes from individual sources, (e.g., $\sim 2-4 \times 10^{-6} \gamma \text{ cm}^{-2} \text{ s}^{-1}$ for the ^{126}Sn 666.3 keV line in Model I with $f_{\text{NSM}} = 100 \text{ Myr}^{-1}$ when integrated over the entire sky), given the larger background, the detection of individual sources may in fact be more favorable.

Several uncertainties affect our predictions. First, we have assumed that each merger produces an r -process abundance distribution following the Solar r abundances for nuclei above mass number $A = 90$. However, detailed analysis of the time evolution of the kilonova spectrum from GW170817 indicated that it contains a lanthanide mass fraction of only $X_{\text{lan}} \sim 10^{-2}$ (e.g., [Kasen](#)

et al. 2017; Kawaguchi et al. 2018), roughly an order of magnitude smaller than that of the solar r abundance pattern above $A = 90$. Future kilonova observations, together with the improved theoretical modeling, as well as the potential late-time detection, may be able to tell whether most of the NSMs produce primarily elements above $A \geq 90$ with a similar amount above the second peak as of the Solar r abundance distribution. If the ^{126}Sn yield in NSM is smaller than what we have assumed, then the prospects of detecting their γ -rays would obviously be correspondingly weaker. On the other hand, one may utilize the fact that ^{126}Sn has three strong lines with clearly predicted energies and branching ratios, to increase the detection confidence in marginal cases.

Our model for the spatial offset distribution of NSM remnants is motivated empirically by observations of short gamma-ray bursts, which are compatible with average center-of-mass velocities of the binary systems of $\sim 20\text{--}140 \text{ km s}^{-1}$. Alternatively, the NSM offsets from their birth site can be modeled on a more physical basis by folding a realistic distribution of SN kick, mass loss during the second SN, stellar motions in different part of MW, the motion of the NS binary under the influence of the MW potential, in addition to the evolution of massive stars in binaries (e.g., Bloom et al. 1999; Belczynski et al. 2006; Chruslinska et al. 2018; Andrews & Zezas 2019). This is beyond the scope of this paper. We note however, that such an approach would necessarily involve large theoretical uncertainties at present but may be improved in the future. For roughly 2/3 of the currently known sample of binary neutron star systems in the MW, the second neutron star appears to have received low kick and low mass ejection, such that they would have negligible change in their center-of-mass velocity. These systems would thus be confined close to the disk and will merge near the Galactic plane (e.g. Beniamini & Piran 2016; Tauris et al. 2017). Nevertheless, the remaining \sim one-third of binary neutron star systems appear to have received relatively high kick velocities (and consequently a large change in center-of-mass velocity). Note that currently it is not possible to ascertain whether the small observed sample is representative of the total population of Galactic neutron star binaries due to the limited sample size and unknown selection bias. The detection of $\gtrsim 10$ NSM remnants with future γ -ray mission proposed here can provide new insights into these open questions.

We encourage further concept studies of various proposed gamma-ray telescope missions, which utilize a range of different detector types, in order to assess their abilities to provide sufficient spatial and energy reso-

lution, as well as a large effective area to achieve the required line sensitivities, as needed to detect NSM remnants in the Milky Way. For example, the germanium detector in COSI and INTEGRAL-SPI demonstrated an excellent energy resolution. The double-sided silicon strip detector proposed in AMEGO and e-ASTROGAM can provide an excellent spatial resolution as successfully demonstrated in Fermi-LAT. A liquid argon time projection chamber (LArTPC) detector proposed in GRAMS can be expanded to a larger scale detector considering that argon is cost effective and widely used in neutrino and dark matter search experiments. A gaseous time projection chamber (TPC) detector in the electron tracking Compton camera (ETCC) is particularly optimized to track Compton scattered electrons, which can further constrain the direction of the incoming γ -ray and reduce coincident background events. The background components on a low-Earth orbit have been well-studied based on the previous experiments and modeled in the energy range of 10 keV to 100 GeV, covering most of the energy range of interest (see e.g., Cumani et al. 2019), but further evaluation will also be needed for each specific mission.

Near the completion of this manuscript, we became aware of independent work on the γ -ray line signals from NSMs, both from extragalactic events and from remnants in the Milky Way (Korobkin et al. 2019). While our work is more specifically focused on Galactic remnants, our conclusions broadly agree with those of these authors.

The authors thank Hsiang-Kuang Chang, Roland Diehl, Enrico Ramirez-Ruiz, Mohammad Safarzadeh, Thomas Siegert, Anna Watts and an anonymous referee for their helpful comments. MRW acknowledges support from the Ministry of Science and Technology, Taiwan under Grant No. 107-2119-M-001-038, and the Physics Division, National Center of Theoretical Science of Taiwan. PB is partly supported by National Natural Science Foundation of China (fund #11533006). BDM acknowledges support from NASA through the Astrophysics Theory Program (grant #NNX16AB30G). GMP is partly supported by the Deutsche Forschungsgemeinschaft (DFG, German Research Foundation) - Projektnummer 279384907 - SFB 1245. TA is supported and funded by Department of Energy (DE-AC02-76SF00515). EB is supported by an appointment to the NASA Postdoctoral Program at the Goddard Space Flight Center, administered by Universities Space Research Association under contract with NASA. CJH acknowledges support from NASA under Contract No. NNG08FD60C. JB is supported by

the National Aeronautics and Space Administration (NASA) through the Einstein Fellowship Program, grant number PF7-180162. GK acknowledges support from the National Science Foundation (grant number

PHY-1404209). MRW and PB thank the Yukawa Institute for Theoretical Physics in Kyoto for support in the framework of the YITP-T-18-06 workshop, during which several aspects of this work have been discussed.

APPENDIX

A. LONG-LIVED NUCLEI AND THEIR DECAY X- AND γ -RAY LINES

Table 2 lists the decay channel, half-life $t_{1/2}$, major lines with intensity larger than 30% for all 22 r -process nuclei that produce decay γ -lines with half-lives between $100 \text{ yr} \leq t_{1/2} \leq 100 \text{ Myr}$. Except for ^{126}Sn , ^{129}I , and ^{182}Hf , all other 19 isotopes are actinides.

In Fig. 7, we show the line fluxes produced from the decay of those nuclei listed in Table 2 at times much shorter than 100 yr. We assume that a NSM at 9 kpc produces an amount of ejecta $M_{\text{ej}} = 0.04 M_{\odot}$. The abundance of ^{126}Sn , ^{129}I , and ^{182}Hf inside the ejecta are assumed to follow the solar r pattern in the same way described in the main text. For the actinides, we assume again, a number fraction of $Y_{\text{act}} = 3.6 \times 10^{-6}$.

B. GALACTIC SN REMNANTS

Fig. 8 shows the distribution of distances, vertical height above the mid-plane of the MW-disk, the Galactic latitude, and longitude for all known SN remnants (excluding Type Ia SNe). This clearly shows that all the SN remnants are located within $\sim \pm 0.5 \text{ kpc}$ from the mid-plane of the Galactic disk and small latitudes within $\sim \pm 5^\circ$, in contrast to the predicted NSM remnant distribution (see Fig. 3). Nevertheless, as mentioned in the main text, it remains possible that some a few SN remnants are in fact from NSMs.

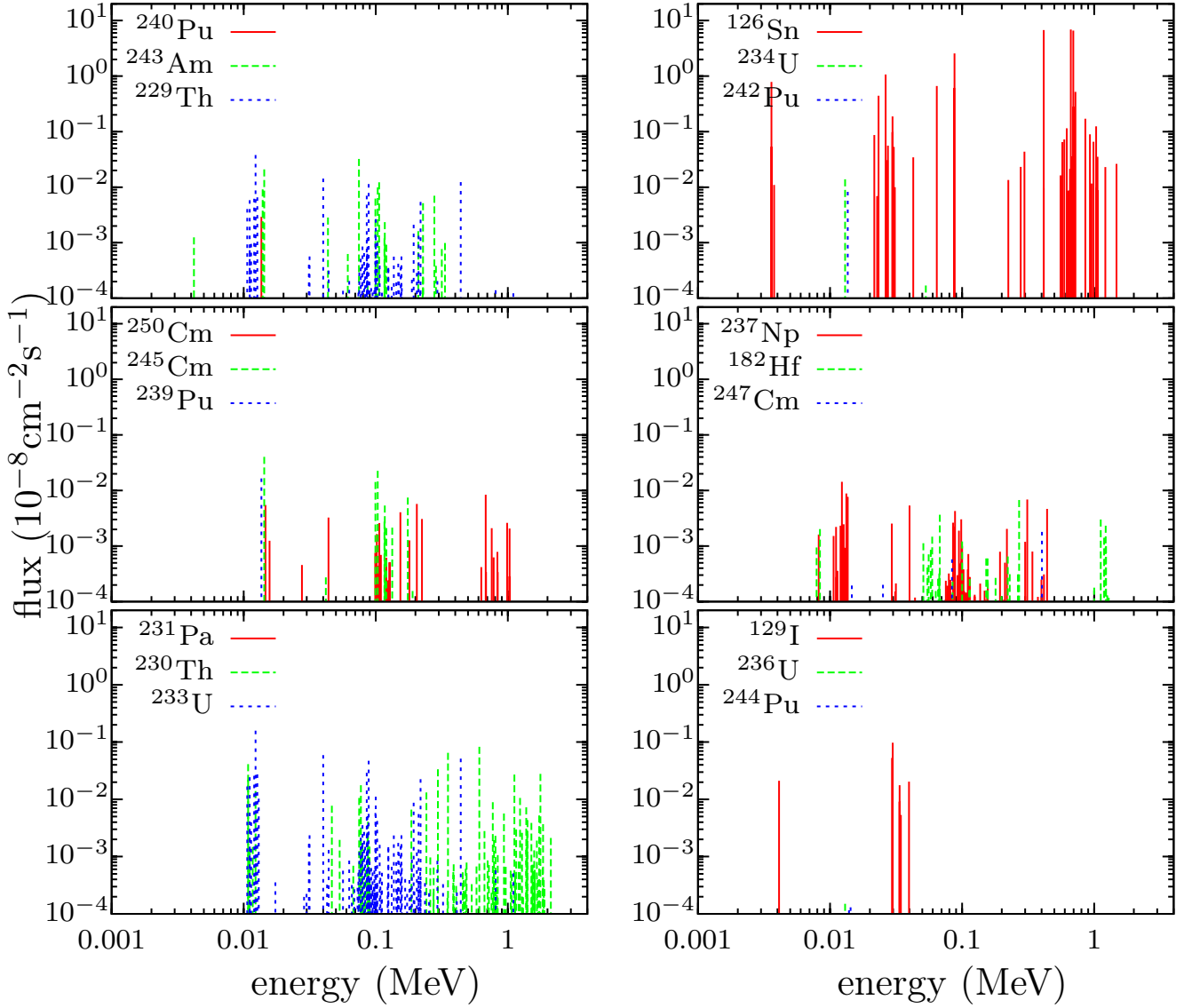


Figure 7. Spectrum of X- and γ -ray line fluxes from a NSM remnant of distance 9 kpc and age 5×10^4 yr (characteristic of the youngest Galactic remnants), including most nuclei from Table 2. The abundance of each isotope is determined as described in the text. Note that the first four nuclei in Table 2 with short half-lives $t_{1/2} < 0.002$ Myr do not contribute fluxes above $10^{-12} \text{ } \gamma \text{ cm}^{-2} \text{ s}^{-1}$ and therefore are not included.

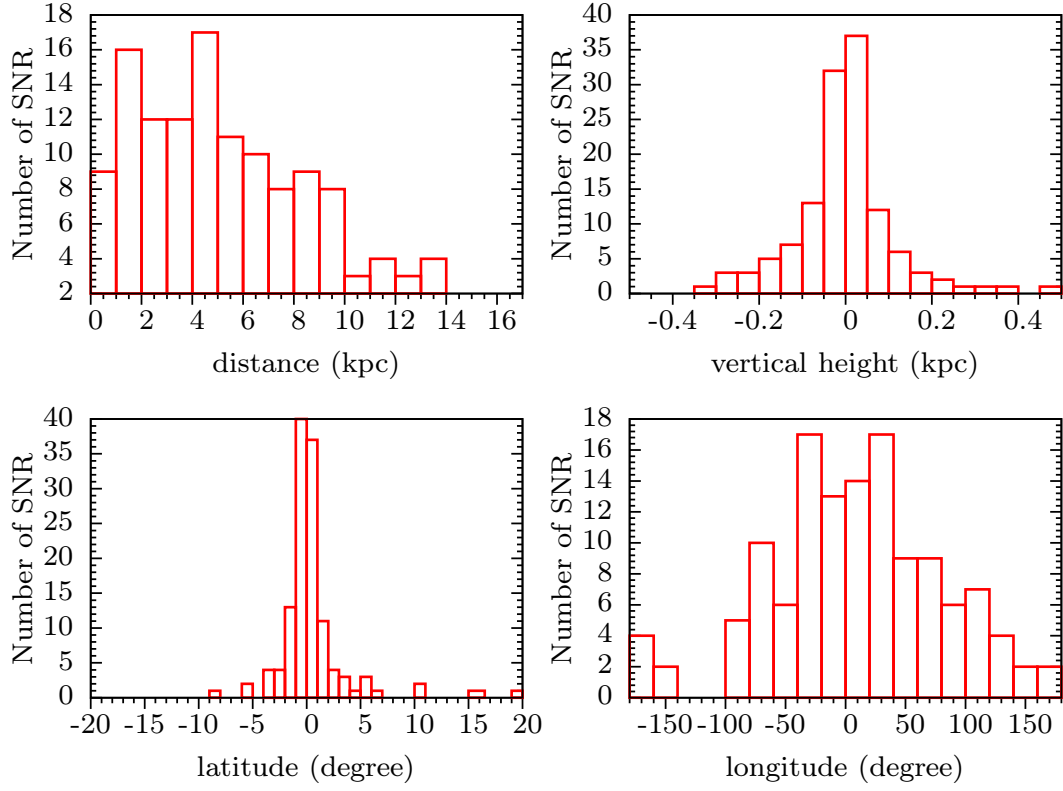


Figure 8. Distribution of the distances, vertical height, latitude, and longitude (in the Galactic coordinate), for known SN remnants. Data taken from [Ferrand & Safi-Harb \(2012\)](#).

Table 2. List of 22 nuclei that produce decay X - and γ -lines with half-lives $100 \text{ yr} \leq t_{1/2} \leq 100 \text{ Myr}$. For lines produced via shorter-lived nuclei inside the decay sequences from a parent isotope, the name of those nuclei are given inside the parenthesis next to the line energy. Note that for each nucleus, only the major lines with line intensities larger than 30%, or the strongest lines (if there is no line with intensity larger than 30%), are listed. The table is compiled from data listed in the NuDat 2 database (NuDat2 2019).

Isotope	Decay channel	$t_{1/2}$ (10^5 yr)	major lines ^a (keV)	intensity $\geq 30\%$
²⁴⁹ Cf	α to ²⁴⁵ Cm	0.0035	388	66.0
²⁴¹ Am	α to ²³⁷ Np	0.0043	13.9 59.5	37.0 35.9
²⁵¹ Cf	α to ²⁴⁷ Cm	0.0090	15	53.0
²²⁶ Ra	$\alpha\beta$ to ²⁰⁶ Pb	0.016	351.9 (²¹⁴ Pb) 609.3 (²¹⁴ Bi)	35.6 45.5
²⁴⁰ Pu	α to ²³⁶ U	0.066	13.6	9.6
²⁴³ Am	$\alpha\beta$ to ²³⁹ Pu	0.074	14.3 (²³⁹ Np) 74.66	43.3 67.2
²²⁹ Th	$\alpha\beta$ to ²⁰⁹ Bi	0.079	12.3 40.0 (²²⁵ Ra)	80.0 30.0
²⁵⁰ Cm	$\alpha\beta$ to ²⁴⁶ Cm	0.083	679.2 (²⁴⁶ Am)	11.5
²⁴⁵ Cm	$\alpha\beta$ to ²³⁷ Np	0.084	14.3	53.0
²³⁹ Pu	α to ²³⁵ U	0.24	13.6	4.3
²³¹ Pa	$\alpha\beta$ to ²⁰⁷ Pb	0.33	12.7	45.0
²³⁰ Th	$\alpha\beta$ to ²⁰⁸ Pb	0.75	351.9 (²¹⁴ Pb) 609.3 (²¹⁴ Bi)	35.6 45.5
²³³ U	$\alpha\beta$ to ²⁰⁹ Bi	1.59	12.3 (²²⁹ Th) 40.0 (²²⁵ Ra)	80.0 30.0
¹²⁶ Sn	β to ¹²⁶ Te	2.3	87.6 414.7 (¹²⁶ Sb) 666.3 (¹²⁶ Sb) 695.0 (¹²⁶ Sb)	37.0 98 100 97
²³⁴ U	α to ²³⁰ Th	2.46	13.0	10.0
²⁴² Pu	α to ²³⁸ U	3.73	13.6	8.6
²³⁷ Np	$\alpha\beta$ to ²⁰⁹ Bi	21.4	12.3 (²²⁹ Th) 13.3 40.0 (²²⁵ Ra) 311.9 (²³³ Pa)	80.0 49.3 30.0 38.5
¹⁸² Hf	β to ¹⁸² W	89	67.7 (¹⁸² Ta) 270.4 1121.3 (¹⁸² Ta)	42.6 79.0 35.24
²⁴⁷ Cm	$\alpha\beta$ to ²³⁵ U	156	14.3 (²³⁹ Np) 74.66 (²⁴³ Am) 402.4	43.3 67.2 72.0
¹²⁹ I	β to ¹²⁹ Xe	157	29.782	36
²³⁶ U	α to ²³² Th	234	13.0	9.0
²⁴⁴ Pu	$\alpha\beta$ to ²³⁶ U	811	14.3 (²⁴⁰ Np) 554.6 (²⁴⁰ Np)	27.0 20.9

^aNote that the lines between 10–20 keV are labeled as XR l in the database and are in fact the aggregation of all L-shell X-ray lines.

REFERENCES

- Abbott, B. P., Abbott, R., Abbott, T. D., et al. 2017a, *Physical Review Letters*, **119**, 161101
- . 2017b, *ApJL*, **848**, L12
- Andrews, J. J., & Zezas, A. 2019, *MNRAS*, **486**, 3213
- Aramaki, T., Hansson Adrian, P., Karagiorgi, G., & Odaka, H. 2019, arXiv e-prints, [arXiv:1901.03430 \[astro-ph.HE\]](#)
- Bargholtz, C., Becker, J., Beshai, S., et al. 1975, *Z. Phys.*, **A**, **272**, 3
- Barnes, J., & Kasen, D. 2013, *ApJ*, **775**, 18
- Belczynski, K., Perna, R., Bulik, T., et al. 2006, *Astrophys. J.*, **648**, 1110
- Beniamini, P., & Piran, T. 2016, *MNRAS*, **456**, 4089
- . 2019, arXiv e-prints, [arXiv:1903.11614 \[astro-ph.HE\]](#)
- Bloom, J. S., Sigurdsson, S., & Pols, O. R. 1999, *Mon. Not. Roy. Astron. Soc.*, **305**, 763
- Boggs, S. E., Harrison, F. A., Miyasaka, H., et al. 2015, *Science*, **348**, 670
- Burbidge, E. M., Burbidge, G. R., Fowler, W. A., & Hoyle, F. 1957, *Rev. Mod. Phys.*, **29**, 547
- Cameron, A. G. W. 1957, *Publ. Astron. Soc. Pac.*, **69**, 201
- Chornock, R., et al. 2017, *ApJL*, **848**, L19
- Chruslinska, M., Belczynski, K., Klencki, J., & Benacquista, M. 2018, *Mon. Not. Roy. Astron. Soc.*, **474**, 2937
- Cioffi, D. F., McKee, C. F., & Bertschinger, E. 1988, *ApJ*, **334**, 252
- Côté, B., Fryer, C. L., Belczynski, K., et al. 2018, *ApJ*, **855**, 99
- Coulter, D. A., Foley, R. J., Kilpatrick, C. D., et al. 2017, *Science*, **358**, 1556
- Cowan, J. J., Sneden, C., Lawler, J. E., et al. 2019, arXiv e-prints, [arXiv:1901.01410 \[astro-ph.HE\]](#)
- Cowan, J. J., Sneden, C., Beers, T. C., et al. 2005, *Astrophys. J.*, **627**, 238
- Cowperthwaite, P. S., Berger, E., Villar, V. A., et al. 2017, *ApJL*, **848**, L17
- Cumani, P., Hernanz, M., Kiener, J., Tatischeff, V., & Zoglauer, A. 2019, *Experimental Astronomy*, **8**
- Diehl, R. 2013, *Reports on Progress in Physics*, **76**, 026301
- Diehl, R., Halluin, H., Kretschmer, K., et al. 2006, *A&A*, **449**, 1025
- Drout, M. R., et al. 2017, *Science*, **358**, 1570
- Eichler, D., Livio, M., Piran, T., & Schramm, D. N. 1989, *Nature*, **340**, 126
- Eichler, M., Sayar, W., Arcones, A., & Rauscher, T. 2019, [arXiv:1904.07013 \[astro-ph.HE\]](#)
- Ferrand, G., & Safi-Harb, S. 2012, *Advances in Space Research*, **49**, 1313
- Fong, W., & Berger, E. 2013, *ApJ*, **776**, 18
- Foucart, F., Hinderer, T., & Nisanke, S. 2018, *PhRvD*, **98**, 081501
- Fryer, C. L., Young, P. A., & Hungerford, A. L. 2006, *ApJ*, **650**, 1028
- Fryer, C. L., et al. 2019, arXiv e-prints, [arXiv:1902.02915 \[astro-ph.HE\]](#)
- Giuliani, S. A., Martnez-Pinedo, G., Wu, M.-R., & Robledo, L. M. 2019, [arXiv:1904.03733 \[nucl-th\]](#)
- Grebenev, S. A., Lutovinov, A. A., Tsygankov, S. S., & Winkler, C. 2012, *Nature*, **490**, 373
- Grefenstette, B. W., Fryer, C. L., Harrison, F. A., et al. 2017, *ApJ*, **834**, 19
- Hirai, Y., Ishimaru, Y., Saitoh, T. R., et al. 2015, *ApJ*, **814**, 41
- Hoffman, R. D., Woosley, S. E., & Qian, Y.-Z. 1997, *ApJ*, **482**, 951
- Holmbeck, E. M., Surman, R., Sprouse, T. M., et al. 2019, *Astrophys. J.*, **870**, 23
- Holmbeck, E. M., Beers, T. C., Roederer, I. U., et al. 2018, *ApJ*, **859**, L24
- Honda, S., Aoki, W., Ishimaru, Y., Wanajo, S., & Ryan, S. G. 2006, *ApJ*, **643**, 1180
- Hotokezaka, K., Beniamini, P., & Piran, T. 2018, *Int. J. Mod. Phys.*, **D27**, 1842005
- Hotokezaka, K., Wanajo, S., Tanaka, M., et al. 2016, *MNRAS*, **459**, 35
- Iyudin, A. F., Diehl, R., Bloemen, H., et al. 1994, *A&A*, **284**, L1
- Ji, A. P., & Frebel, A. 2018, *ApJ*, **856**, 138
- Ji, A. P., Frebel, A., Chiti, A., & Simon, J. D. 2016, *Nature*, **531**, 610
- Kasen, D., Metzger, B., Barnes, J., Quataert, E., & Ramirez-Ruiz, E. 2017, *Nature*, **551**, 80
- Kawaguchi, K., Shibata, M., & Tanaka, M. 2018, *ApJL*, **865**, L21
- Kierans, C. A., et al. 2016, *PoS, INTEGRAL2016*, 075
- Kim, C., Kalogera, V., & Lorimer, D. 2010, *New Astronomy Reviews*, **54**, 148
- Korobkin, O., Rosswog, S., Arcones, A., & Winteler, C. 2012, *Mon. Not. R. Astron. Soc.*, **426**, 1940
- Korobkin, O., et al. 2019, [arXiv:1905.05089 \[astro-ph.HE\]](#)
- Krause, M. G. H., Diehl, R., Bagetakos, Y., et al. 2015, *Astron. Astrophys.*, **578**, A113
- Lattimer, J. M., & Schramm, D. N. 1974, *Astrophys. J. Lett.*, **192**, L145
- Li, L.-X. 2019, *ApJ*, **872**, 19
- Li, L.-X., & Paczyński, B. 1998, *ApJL*, **507**, L59
- Limongi, M., & Chieffi, A. 2006, *ApJ*, **647**, 483
- Lorimer, D. R. 2008, *Living Reviews in Relativity*, **11**, 8

- Madsen, K. K., Harrison, F., Broadway, D., et al. 2018, in *Society of Photo-Optical Instrumentation Engineers (SPIE) Conference Series*, Vol. 10699, *Space Telescopes and Instrumentation 2018: Ultraviolet to Gamma Ray*, 106996M
- Margalit, B., & Metzger, B. D. 2019, [arXiv:1904.11995 \[astro-ph.HE\]](#)
- McMillan, P. J. 2017, *MNRAS*, **465**, 76
- Metzger, B. D., Quataert, E., & Thompson, T. A. 2008, *Mon. Not. Roy. Astron. Soc.*, **385**, 1455
- Metzger, B. D., Thompson, T. A., & Quataert, E. 2007, *Astrophys. J.*, **659**, 561
- Metzger, B. D., Martínez-Pinedo, G., Darbha, S., et al. 2010, *Mon. Not. R. Astron. Soc.*, **406**, 2650
- Meyer, B. S., Mathews, G. J., Howard, W. M., Woosley, S. E., & Hoffman, R. D. 1992, *ApJ*, **399**, 656
- Miller, M. J., & Bregman, J. N. 2013, *ApJ*, **770**, 118
- Miller, R. S., Ajello, M., Beacom, J. F., et al. 2018, in *LPI Contributions*, Vol. 2063, *Deep Space Gateway Concept Science Workshop*, 3094
- Moiseev, A., & Team, O. B. O. T. A. 2018, *PoS, ICRC2017*, 798
- Montes, G., Ramirez-Ruiz, E., Naiman, J., Shen, S., & Lee, W. H. 2016, *Astrophys. J.*, **830**, 12
- Mösta, P., Roberts, L. F., Halevi, G., et al. 2018, *ApJ*, **864**, 171
- Nandra, K., Barret, D., Barcons, X., et al. 2013, arXiv e-prints, [arXiv:1306.2307 \[astro-ph.HE\]](#)
- NuDat2. 2019, National Nuclear Data Center, information extracted from the NuDat 2 database, <http://www.nndc.bnl.gov/nudat2>
- Olausen, S. A., & Kaspi, V. M. 2014, *ApJS*, **212**, 6
- Orth, C. J., Dropesky, B. J., & Freeman, N. J. 1971, *Phys. Rev. C*, **3**, 2402
- Pian, E., et al. 2017, *Nature*, **551**, 67
- Plüschke, S., Diehl, R., Schönfelder, V., et al. 2001, in *ESA Special Publication*, Vol. 459, *Exploring the Gamma-Ray Universe*, ed. A. Gimenez, V. Reglero, & C. Winkler, 55
- Qian, Y., & Woosley, S. E. 1996, *Astrophys. J.*, **471**, 331
- Qian, Y.-Z., Vogel, P., & Wasserburg, G. J. 1998, *ApJ*, **506**, 868
- . 1999, *ApJ*, **524**, 213
- Ray, P. S., et al. 2018, *Proc. SPIE Int. Soc. Opt. Eng.*, **10699**, 1069919
- Renaud, M., Vink, J., Decourchelle, A., et al. 2006, *ApJL*, **647**, L41
- Ripley, J. L., Metzger, B. D., Arcones, A., & Martínez-Pinedo, G. 2014, *MNRAS*, **438**, 3243
- Safarzadeh, M., Ramirez-Ruiz, E., Andrews, J., et al. 2019, *Astrophys. J.*, **872**, 105
- Schoenfelder, V., Aarts, H., Bennett, K., et al. 1993, *ApJS*, **86**, 657
- Shen, S., Cooke, R. J., Ramirez-Ruiz, E., et al. 2015, *Astrophys. J.*, **807**, 115
- Siegel, D. M., Barnes, J., & Metzger, B. D. 2019, *Nature*, **569**, 241
- Siebert, T., Diehl, R., Krause, M. G. H., & Greiner, J. 2015, *A&A*, **579**, A124
- Sieverding, A., Martínez-Pinedo, G., Huther, L., Langanke, K., & Heger, A. 2018, *Astrophys. J.*, **865**, 143
- Smith, D. M. 2004, in *ESA Special Publication*, Vol. 552, *5th INTEGRAL Workshop on the INTEGRAL Universe*, ed. V. Schoenfelder, G. Lichti, & C. Winkler, 45
- Smith, H. A., Bunker, M. E., Starner, J. W., Orth, C. J., & Löbner, K. E. G. 1976, *Phys. Rev. C*, **13**, 387
- Snedden, C., Cowan, J. J., & Gallino, R. 2008, *Annu. Rev. Astron. Astrophys.*, **46**, 241
- Soares-Santos, M., et al. 2017, *ApJL*, **848**, L16
- Symbalisty, E., & Schramm, D. N. 1982, *Astrophys. J. Lett.*, **22**, 143
- Takahashi, K., Witt, J., & Janka, H.-T. 1994, *Astron. Astrophys.*, **286**, 857
- Tanaka, M., & Hotokezaka, K. 2013, *ApJ*, **775**, 113
- Tanimori, T., et al. 2017, *Sci. Rep.*, **7**, 41511
- Tanvir, N. R., et al. 2017, *ApJL*, **848**, L27
- Tauris, T. M., Kramer, M., Freire, P. C. C., et al. 2017, *ApJ*, **846**, 170
- Tavani, M., et al. 2018, *JHEAp*, **19**, 1
- The LIGO Scientific Collaboration, & the Virgo Collaboration. 2018, arXiv e-prints, [arXiv:1811.12907](#)
- Thompson, T. A., Burrows, A., & Meyer, B. S. 2001, *Astrophys. J.*, **562**, 887
- Thompson, T. A., Chang, P., & Quataert, E. 2004, *Astrophys. J.*, **611**, 380
- Tur, C., Heger, A., & Austin, S. M. 2010, *ApJ*, **718**, 357
- van de Voort, F., Quataert, E., Hopkins, P. F., Kereš, D., & Faucher-Giguère, C.-A. 2015, *MNRAS*, **447**, 140
- Villar, V. A., Guillochon, J., Berger, E., et al. 2017, *ApJL*, **851**, L21
- Vink, J. 2012, *A&A Rv*, **20**, 49
- Vink, J., Laming, J. M., Kaastra, J. S., et al. 2001, *ApJL*, **560**, L79
- Vlasov, A. D., Metzger, B. D., Lippuner, J., Roberts, L. F., & Thompson, T. A. 2017, *MNRAS*, **468**, 1522
- Wanajo, S. 2018, *ApJ*, **868**, 65
- Wang, W., Harris, M. J., Diehl, R., et al. 2007, *A&A*, **469**, 1005
- Wehmeyer, B., Pignatari, M., & Thielemann, F.-K. 2015, *MNRAS*, **452**, 1970

- Winteler, C., Käppeli, R., Perego, A., et al. 2012, [Astrophys. J. Lett.](#), **750**, L22
- Woosley, S. E., Wilson, J. R., Mathews, G. J., Hoffman, R. D., & Meyer, B. S. 1994, [Astrophys. J.](#), **433**, 229
- Wu, M.-R., Barnes, J., Martínez-Pinedo, G., & Metzger, B. D. 2019, [Physical Review Letters](#), **122**, 062701
- Wu, M.-R., Banerjee, P., Metzger, B. D., et al. 2019, supplemental data: possible Sn126 decay gamma-ray fluxes from known SNRs and magnetars, v1.0, Zenodo, <https://doi.org/10.5281/zenodo.3228556>
- Xue, Y. Q., et al. 2019, [Nature](#), **568**, 198
- Zhang, S. N., et al. 2016, [Proc. SPIE Int. Soc. Opt. Eng.](#), **9905**, 99051Q
- Zhu, Y., Wollaeger, R. T., Vassh, N., et al. 2018, [ApJL](#), **863**, L23